Stem Cell Reports, Volume *12*

Supplemental Information

Visualizing the Contribution of Keratin-14^{+} Limbal Epithelial Precursors in Corneal Wound Healing

Mijeong Park, Alexander Richardson, Elvis Pandzic, Erwin P. Lobo, Renee Whan, Stephanie L. Watson, J. Guy Lyons, Denis Wakefield, and Nick Di Girolamo

Supplementary Figures and Text

Figure S1

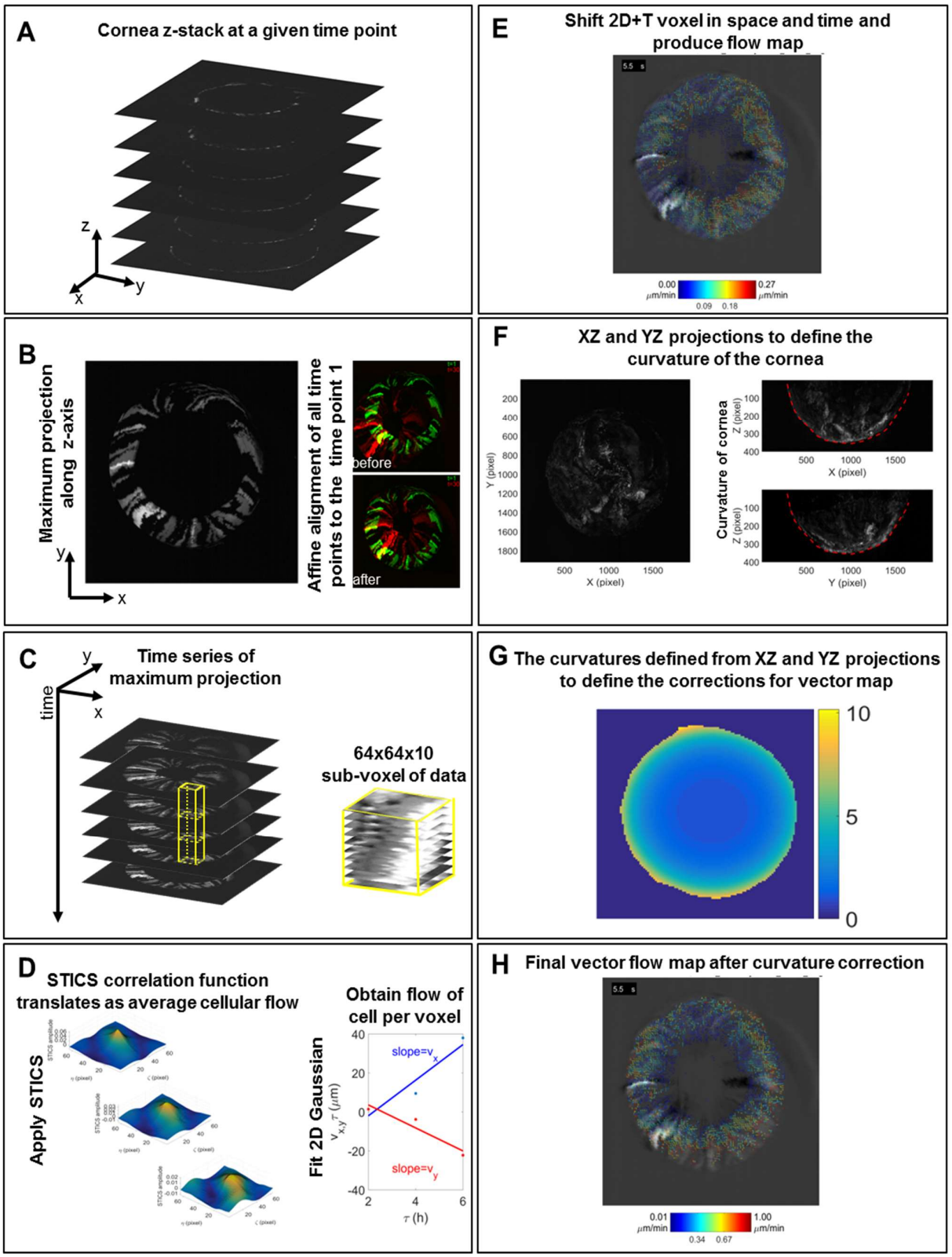

Supplementary Figure Legend

Figure S1: Spatio-Temporal Image Correlation Spectroscopy (STICS) pipeline

(A) Cornea Z-stacks were acquired every 2 hrs for 48 hrs from *ex vivo* organ-cultured corneas using light-sheet microscopy. (B) The maximum intensity projection (MIP) was calculated along the Z-axis for every time point and MIPs from all four channels were merged to produce a single gray-scale time series in the X-Y plane. Every time point in the series was then aligned to the first time point. (C) STICS was applied on the registered time series of MIP; 64×64 pixels by 10 frames. (D) STICS correlation function was calculated using a fast fourier transform, and fitted by a 2D Gaussian function at each time lag, and peak positions were further linear-fitted to extract the flow vector (velocities in X and Y directions; v_x, v_y) for each voxel. (E) An example of full velocity vector map for an early time point. Blue to red arrows indicate increase in velocity. (F) The cornea curvature is measured on X-Z and Y-Z projections of Z-stacks. (G) The correction vector map is calculated from the curvature traces. (H) Correction map is multiplied to correct the velocity map from (E) to account for the difference in clonal displacement along corneal curvature.

Supplementary Tables

Table S1. Basal epithelial cell dimension and epithelial thickness adjacent the wound margin in 2 mm central wounds, related to Figure 1B.

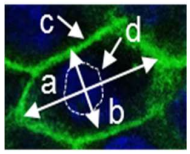	**Size of cells** (axis; µm)		**Perimeter** (µm)		**Cell density** (425×425µm)	**Epithelial thickness** (µm)
	Maximum (a)	Minimum (b)	Cell (c)	Nuclei (d)		
Wound	15.5 ± 2.0	10.3 ± 0.6	46.2 ± 5.1	28.3 ± 2.4	1608.3 ± 444.6	12.0 ± 0.7
Control	11.5 ± 1.1	7.1 ± 0.4	34.3 ± 2.6	25.1 ± 1.9	3131.3 ± 593.2	18.2 ± 0.8
***p* value**	0.0198 (*)	0.0003 (***)	0.0113 (*)	0.15 (ns)	0.0117 (*)	<0.0001 (****)

*Seven-wk-old WT mice had their right corneal epithelium debrided to create a 2 mm central wound. Average measurement of each parameter was obtained from PFA-fixed and flat-mounted phalloidin-stained corneas at 16 hrs post-injury by scanning confocal microscopy. Data represent mean ± SD, n=4/group, *p<0.05, ***p< 0.001, ****p< 0.0001, ns = p>0.05 using an unpaired two-tailed Welch's t-test.*

Table S2. Average size of basal epithelial cells from simulated corneas, related to Figure 6 and Video 4.

	Relative to cell area		
	Peripheral cells	**Intermediate cells**	**Central cells**
Wound	1.04 ± 0.03	1.05 ± 0.03	1.04 ± 0.04
Control	1.0 ± 0.04	1.0 ± 0.05	1.0 ± 0.06
***p* value**	0.0007 (***)	0.0006 (***)	0.0116 (*)

*The average size of the basal cells was significantly increased in the central region compared to peripheral and intermediate zones Data represent mean ± SD, n=20/group, *p<0.05, ***p< 0.001, ****p< 0.0001 by repeated measures (2300 time unit) one-way ANOVA with Sidak multiple comparisons correction.*

Supplementary Experimental Procedures

Histological assessment

Mice were sacrificed by cervical dislocation at specific time points post-wounding. Eyes were enucleated, fixed in 10% neutral buffered formalin overnight at room temperature (RT), then placed in 70% ethanol. Corneas were procured from intact globes and bisected prior to embedding in agarose then paraffin; this ensured correct orientation relative to the wound. Tissue sections (4 µm) were cut, dewaxed and rehydrated prior to staining with hematoxylin and eosin (H&E) or periodic acid Schiff (PAS). They were mounted in DPX mounting medium (Sigma-Aldrich), observed under a BX51 light microscope (Olympus, Center Valley, PA), imaged on a digital camera (DP73; Olympus) and processed using CellSens® (Olympus).

Immunofluorescence

To confirm the phenotype of the regenerated epithelium, mice were euthanized at specific time points post-wounding, eyes were enucleated and fixed in 10% neutral buffered formalin, and corneas dissected and paraffin-embedded. Antigen retrieval was performed by placing slides in Target Retrieval™ (Dako, Glostrup, Denmark) solution for 5 min at 110°C in a NxGen® Decloaking Chamber (Biocare Medical, Pacheco, CA). Sections were equilibrated in Tris-buffered saline (TBS, pH 7.6) then blocked in 20% goat or rabbit serum diluted in TBS containing 2% bovine serum albumin (TBS-B) (Sigma-Aldrich) for 1 hr at RT. Next, they were incubated for 2 hrs at RT with a pre-determined concentration of primary antibody (Ab) including goat anti-K12 (2 µg/ml; sc-17101; Santa Cruz, Dallas, TX), goat anti-K13 (2 µg/ml; sc-31703; Santa Cruz), rabbit anti-K14 (1 µg/ml; GTX104124; GenTex, San Antonio, TX) and rat anti-K8/18 (2 µg/ml; TROMA-I; DSHB, Iowa City, IA) in TBS-B. Abs to rabbit (Santa Cruz), goat (Santa Cruz) and rat (Life Technologies, Carlsbad, CA) IgG were used as reagent negative controls. Sections were flooded with TBS to

remove unbound Abs, then reacted with Alexa-Fluor^{488}-conjugated rabbit anti-goat, Alexa-Fluor^{647}-conjugated chicken anti-rabbit or Alexa-Fluor^{488}-conjugated goat anti-rat secondary Abs (Life Technologies) in TBS-B at a final concentration of 5 µg/ml for 45 mins at RT. Sections were mounted in ProLong Gold® anti-fade containing DAPI (Life Technologies), viewed under a BX51 fluorescence microscope (Olympus), images taken on a DP73 digital camera (Olympus) and processed using CellSens® (Olympus). For K12/K14 double-staining, images were acquired on a Zeiss 780 confocal microscope (Carl Zeiss).

Measuring clonal migration and wound closure by intra-vital microscopy

Anaesthetized Confetti and WT mice were placed under a 3i VIVO™ fluorescence microscope (Intelligent Imaging Innovations, Denver, CO), and wide-field images acquired using 4 filters compatible for CFP, GFP, YFP and RFP to record the status of the ocular surface prior to wounding; CFP 458 nm excitation, 464-495 nm emission; GFP 488 nm excitation, 497-510 nm emission; YFP 514 nm excitation, 517-540 nm emission; RFP 561 nm excitation, 575-654 nm emission. A droplet (25 µl) of 0.1% sodium fluorescein (Minims, iNova Pharmaceuticals, Sydney, Australia) was instilled for 5 sec, each eye was rinsed with 5 ml of PBS, then corneas imaged again. At selective time points, corneas were assessed by intravital microscopy using a 2.5×/0.085 detection lens, images were taken and processed using SlideBook v.6 (3i Intelligent Imaging Innovations, https://www.intelligent-imaging.com) and ImageJ software (NIH, https://imagej.nih.gov/ij) (Abràmoff et al., 2004; Cruzat et al., 2011). Wound closure rate was estimated from measurements taken after applying fluorescein. Clonal migration in Confetti mice was estimated by measuring the length of 5 or more limbal-originating streaks of each color over time, and the rate expressed as µm/hr (Di Girolamo et al., 2015; Lobo et al., 2016; Richardson et al., 2017). At least 3 mice were used per group/time point. Due to the elevated K14^{+} clonal migration during wound-healing and due to the limited amount of ketamine animals could endure over this period, two groups of mice were established in which the monitoring period was offset. Live Confetti mice in Group 1 were inspected at 0 hrs, 8 hrs, 24 hrs and 72 hrs, and those in Group 2 at 0 hrs, 16 hrs, 48 hrs and 72 hrs post-injury.

Confocal microscopy

Confetti transgenic mice were euthanized at designated time points post-wounding, eyes were enucleated, fixed in 4% paraformaldehyde overnight at 4°C, then placed in PBS prior to experimentation. Corneas were procured, extraneous tissues (lens, iris, retina and ocular muscles) removed and imaged by confocal fluorescence microscopy (Zeiss LSM 780; Carl Zeiss) with a 20×/0.8 or 100×/1.4 detection lens. The four fluorescent protein signatures were collected sequentially as follows; CFP 458 nm excitation, 455-499 nm emission; GFP 488 nm excitation, 490-508 nm emission; YFP 514 nm excitation, 517-544 nm emission; RFP 561 nm excitation, 579-659 nm emission. Four relaxing radial

incisions were made on the corneas to facilitate flat-mounting. Corneas were placed epithelial side-down on glass slides, mounted in ProLong Gold® anti-fade reagent containing DAPI (Life Technologies), weighted overnight to facilitate flattening, and imaged using a Zeiss 780 confocal microscope (Carl Zeiss). To capture the entire sample, 121 frames were merged into a single 11×11 tiled image. Z-stack images were collected, merged using a maximum intensity projection with Zen (Carl Zeiss), then analyzed with ImageJ software. The number of fluorescent stripes was determined by manually counting each as they emerged from limbal margin. Clone width at the periphery was estimated (using a scale bar as a reference) from at least 10 fluorescent streaks comprising YFP and RFP (Richardson et al., 2017).

Spatio-Temporal Image Correlation Spectroscopy of clonal migration in ex vivo wounded corneas

As an alternative and more accurate means of measuring cell movement, Spatio-Temporal Image Correlation Spectroscopy (STICS) (Toplak et al., 2012; Meddens et al., 2016; Ashdown et al., 2017) was applied on a series of 2D maximum intensity projections of 3D image stacks that were acquired via light-sheet microscopy (Zeiss Lightsheet Z.1; Carl Zeiss, Jena, Germany) at different time points post-injury in *ex vivo* organ-cultured murine corneas. The raw data consisted of a temporal sequence (i.e. time point per 2 hrs) of Z-stacks from corneas imaged through a 5×/0.16 detection lens and 5×/0.1 illumination lens (pixel size 2.28 µm). The four fluorescent protein signatures were collected sequentially as follows; CFP 445 nm excitation, 460-500 nm emission; GFP 488 nm excitation, 505-545 nm emission; YFP 514 nm excitation, 525-545 nm emission; RFP 561 nm excitation, 575-654 nm emission. Z-stack images were collected with an optimal sectioning step of 4.35 µm (proximally 550 slices). For every time point (Figure S1A), the maximum intensity projection image was calculated along the Z-axis (Figure S1B). Although the data was acquired in four channels, all intensities were combined to produce a single grayscale time series of maximum projection images in the X-Y plane (Figure S1C). Image registration (Figure S1B; images superimposed) was performed using image cross-correlation; this ensured alignment of every frame in the series to the first. STICS was then applied on the registered maximum intensity projection time series, where the local region of interest was set to 64×64 pixels by 10 frames (Figure S1C; data sub-voxel). Registered image series were Fourier filtered to exclude immobile components as previously described (Toplak et al., 2012). For each voxel of data, STICS correlation function (CF) was calculated (Figure S1C, 3 temporal lags CF; yellow colored rectangular prism). CF is the fit with a 2D Gaussian function at each temporal lag, and the peak positions were further fitted to extract the flow vector (v_x, v_y) for each voxel (Figure S1D). The spatial shift of 16 pixels in X and Y plane ensured over-sampling between adjacent regions which was used to filter out erroneous flows. Briefly, the mean of 8 nearest neighbouring region speeds were compared to the central region value and if outside the variance of the neighbourhood, the value was set to a not-a-number. To achieve the temporal evolution of flow-map, 10 frames at a time were analyzed and the temporal block of images shifted by 1 frame (2 hrs)

to ensure continuous transition in flow per region of interest, and to also account for possible change in local flow during the experiment. The resulting vector flow-map was obtained as result of spatio-temporal shift of data sub-voxel (Figure S1E). Furthermore, to account for the 3D cellular movement on the surface of cornea, its curvature was measured on the X-Z and Y-Z projections of the Z-stack (Figure S1F, red hatched lines). From the curvature traces, the correction map was calculated (Figure S1G) which was used to correct the flow-map obtained from maximum projections in X-Y plane (Figure S1E); this was subsequently converted into a vector flow-map of cells produced from the movement on the curved surface defined by the cornea (Figure S1H). The corrected spatio-temporally resolved vector flow-maps were further analyzed by combining the speed of cells at the leading edge of the wound, and their histograms compared to those obtained for speed in the peripheral region. These analyses were conducted in custom built software MATLAB (MathWorks, Natik, MA).

Overview, design concepts and details of the mathematical model

1. Purpose

The model is used to investigate the role that population pressure-driven motility plays in corneal wounding and repair and to compare spatial distributions of clonally related cells in corneas, following cases of no wounding and wounding in a central circular format. It is based on a previous model (Grimm et al., 2010; Lobo et al., 2016).

2. Entities, state variables and scales

The model space is a circular region representing the cornea and adjacent limbus, which collectively is in one of three states: a 'healthy state', an 'early wounded state' and a 'late wounded state'. The healthy state represents a cornea whose dynamics do not incorporate any wound, or any active response to previous wounding. The early wounded state represents a cornea that is undergoing repair, where the key driver of wound repair is cell movement into the vacant wounded area, before the wound approaches closure. The late wounded state represents a cornea that has almost transitioned into the healthy state, where the key component of wound repair is cells coming together spatially, which results in wound closure.

Regardless of collective state of the cornea, the model consists of approximately 4,000 cells within the basal layer inside a circular perimeter with a diameter of 115 idealized cell radii (defined below in '*5. Initialization*'). Each cell has the following attributes or state variables:

1. Position: The position of a cell is determined by a single pair of co-ordinates, as we ignore the curvature of the basal layer of the cornea. Collectively, the set of cell positions is used to determine the edges and vertices of cells,

using geometric structures known as Voronoi diagrams. We assume the limbus consists exclusively of stem cells, which are all within a single cell rim, a fixed distance away from the center of the corneal region.

2. Lineage identification: Each stem cell is endowed with a distinct lineage identification code, and all future progeny of that stem cell in the cornea share the same cell lineage identification code.

3. Age: Cells are attributed with a current age. Processes such as time to cell death, symmetric cell division and differentiation off the basal layer are assumed to occur approximately periodically.

4. Type: Each cell is characterized by a type that is used to reflect the phenotypic behavior of cells in the cornea, or to maintain the model. Cell types include: Ghost cells, whose position is exterior to the circular region that represents the cornea, and are designed to play no active part in corneal dynamics, but are necessary to maintain the spatial structure of the model; Blank cells, that represent wounded areas inside the circular region that are not occupied by other cell types; epithelial stem cells that represent the phenotypic properties of stem cells found in the limbus otherwise known as LESCs; and TACs within the cornea. An injury transforms cells in the wounded area from TAC cells into Blank cells and moves the cornea from a healthy state to an early wounded state.

5. Cell types Blanks, LESC and TAC differ in the following way depending on the collective state:

5.1. Healthy state

	Blank [a]	**LESC**	**TAC**
Lifespan	n/a	Normally distributed N (3000, 10)	Normally distributed N(300, 10)
Replicative capacity	n/a	∞ [b]	TAC(max) = 3 [c]
Replicative Frequency	n/a	R^* [d]	N(300, 10) [e]

a) Blank cells are not present in the healthy state

b) LESCs are assumed to have a replicative capacity that is much greater than the time scale represented by the model and are therefore characterized by limitless replicative potential for both symmetric and asymmetric proliferation in the model. LESCs are assumed to replicate symmetrically, producing two LESCs, or asymmetrically, producing an LESCs and a TAC

c) TACs can divide asymmetrically to produce another TAC and a TDC. TDCs do not contribute to the basal layer and are not depicted in simulations. TACs have a limited number of rounds of symmetric cell division, known as TAC(max), after which they divide symmetrically to produce two TDCs.

d) The value of R^*, the replicative rate of LESC's are chosen to maintain equilibrium in cell population over time. This is determined by the model parameters and depends on the other parameters listed above.

e) At the end of their lifespan, TAC(n) cells divide symmetrically to produce two TAC(n-1) cells when $n>1$, or two TDC cells when $n=1$.

5.2 Early and late wounded state

	Blank	**LESC**	**TAC**
Lifespan	Dependent on properties of the Blank cell [a]	Normally distributed $N(3000, 10)$	Normally distributed $N(300, 10)$
Replicative capacity	None	∞	TAC(max) = 3
Replicative Frequency	n/a	$2.5R^*$ [b]	$N(300, 10)$

a) In the early wounded state, cells in the circular region more effectively push into Blank cells than other cells in the cornea. This represents the preference for cells to move into unoccupied wounded areas of the cornea over competing for space with other cells. Blank cells remain in the cornea and may occupy less of the basal layer, but they are not yet removed. In the late wounded state, Blank cells are removed as follows:

b) Blank cells are further classified as internal Blank cells, which are only adjacent to other Blank cells, and edge Blank cells, which are adjacent to at least one TAC cell.

- When the distance between two internal Blank cells is small enough (less than 0.15 idealized cell radii), they are replaced by a single Blank cell whose position takes the value of the average position of the two internal cells being replaced
- The cornea moves from an early wounded state to a late wounded state when there are more edge Blank cells than internal Blank cells. When the cornea is in the late wounded state, Blank cells are removed stochastically with $p = 0.2$ per Blank cell per time step, and are not replaced.

c) LESCs have a 2.5-fold increase in proliferation as a response to wounding.

3. Processes overview and scheduling

At each step, the following processes occur in this order:

1. Cell motility
2. Possible wounding and changing the collective state to one of healthy, early wounding or late wounding
3. Remove Blank cells if in late wounding state
4. Render and record the state of the simulation
5. Cell division of LESCs
6. Differentiation off the basal layer
7. Cell division of TACs

4. Design Concepts

1. Basic principles: We make the following assumptions
   a) The cornea is in a state of homeostasis, conforming with the X, Y, Z hypothesis (Thoft and Friend, 1983).
   b) The cell lineage pathways in the cornea are LESC-TAC-TDC
   c) There is a fixed population of LESCs in the limbus
   d) The cells in the cornea are motile
   e) The population pressure is related to the density of neighboring cells
   f) Cells respond to pressure gradients by moving from higher pressure to lower pressure areas.
   g) TAC cells preferentially move to the direction of an adjacent Blank cell rather than other TACs or LESCs.
2. Emergence: the spatial structures of cell lineages in the cornea emerge through passive motility rules, driven by a cellular spring network.
3. Adaptation: cells in the cornea move in response to the pressure exerted by their immediate neighbors and either replicate or die in response to reaching their lifespan; LESCs respond to the death of a neighbor by replicating themselves; these responses do not adapt over time or in response to position.
4. Objectives: the cells do not aim to meet any objectives.
5. Learning: individual cells do not change their adaptive traits over time in response to experience.
6. Prediction: there are no adaptive traits in the model, so the agents in the model do not make any predictions.
7. Sensing: cells can sense the pressure exerted by their neighbors and whether they are located in the limbus or the cornea. Blank cells can sense whether their neighbors are TACs or other Blank cells.
8. Interaction: cells respond to the local configurations of other cells by moving in response to a pressure gradient or, in the case of LESCs, replicating in response to the death of a neighbor.

9. Stochasticity: the lifespans of cells are normally distributed for both LESCs and TACs. The other source of stochasticity in the model occurs when a neighboring LESC is elected to undergo symmetric cell division in response to the removal (death) of a LESC.

10. Collectives: there is no pre-determined collective behavior in the model.

11. Observation: position, lineage identification code, age and proliferative capacity are recorded for all cells in the model at every time step.

5. Initialization

Cell positions are initially chosen so that the Voronoi diagram generated is a regular hexagonal grid (the distance between the positions of neighboring cells is a constant, *s*, known as the idealized cell diameter). All LESCs are given a random age (uniformly distributed from 0 to their lifespan) and a unique cell lineage identification code. Initially, all TACs are not assigned a lineage identification code. TACs derived from LESCs after initialization inherit the lineage identification code of their parent cell. Cell types are chosen such that LESCs have only two adjacent LESC neighbors, and that TACs that have less proliferative capacity are placed towards the center of the cornea. The model is run for 2000 pre-simulation time steps to achieve homeostasis. At this point, all cells have acquired a lineage identification code, and a stable spoke-like pattern has been achieved, and the simulation begins.

6. Input

There are no external input data that alter the model during the simulations.

7. Sub-models

Cell motility in response to pressure: the cell positions of all TACs are updated through a cell movement rule, which is applied 100 times per time step. Each time the movement rule is applied, the set of Voronoi neighbors (found through Delaunay Triangulation) is found, and cell movement arising from pressure between a TAC neighboring cell is proportional to the d_p-s_t, where d_p represents the distance between the cell neighbors, and s_t varies depending on the types of cells that are neighbors as follows:

Cell type	**Neighboring cell type**	$\mathbf{S_t}$

LESCs or TACs	LESCs or TACs	s^a
TACs	Blank	$0.95\ s^b$
Blank	TACs	$1.05s^b$
Blank	Blank	s_b^c

a) s is the idealized cell diameter

b) TACs preferentially move towards vacant areas of the cornea, and Blank cells in the wounded area move away from this advancing frontier

c) s_b is determined dynamically to be the average Blank cell diameter that covers the current area of wound

The total movement of a cell is the sum of all movements arising from each pair of neighbors, and this is done synchronously. The positions of both LESCs and Ghosts are fixed.

1. Cell motility: Cell positions are updated through the following movement rule which is applied 100 times per time step

$$\Delta p_i = \frac{1}{2\sqrt{3}} \sum_j w_{i,j}(p_i - p_j)\left(s_t - |p_i - p_j|\right)/|p_i - p_j|$$

2. Render and record the state of the simulation, collect all figures and data.

3. Age cells: All cells are assumed to age synchronously.

4. LESCs that have reached their lifespan are removed and are synchronously replaced by symmetric proliferation of a neighboring LESC, which is chosen at random. The cell lineage identification of the new cell matches that of the mother cell, and the lifespan of the new cell is chosen randomly from N (3000, 10).

5. LESCs give rise to TAC(max)s at a rate designed to maintain corneal equilibrium. Newly proliferated TACs share the lineage identification of the mother cell, its position is 0.5s closer to the center of the cornea than the mother cell, and the lifespan of the TAC(max) is chosen randomly from N (75, 25). While the cornea is wounded, this rate is increased 2.5-fold.

6. When $s_b^c < 0.15s$, Blank cells are considered to be sufficiently small, are completely surrounded by other Blank cells (known as internal Blank cells) and are deemed to be available for removal. Blank cells that are within 0.25s to another Blank cell are removed leaving a singular, larger Blank cell. When there are no internal Blank cells, the remaining Blank cells are removed stochastically with $p = 0.2$ per Blank cell per time step.

7. Cell differentiation off the basal layer: TACs that have reached their lifespan and exhausted their replicative

potential die by becoming TDCs in the suprabasal layers of the epithelium and are removed from the model.

8. Symmetric division of a TAC with *x* rounds of cell division remaining produces two daughter TACs, both having *x-1* potential rounds of cell division remaining. Both these daughter cells share the lineage identification code as the mother cell and are placed within 0.5s of the position of the mother cell, with no other predetermined spatial assignment.

Supplementary References

Abràmoff, M.D., Magalhães, P.J., and Ram, S.J. (2004). Image processing with ImageJ. Biophotonics international *11*, 36-42.

Ashdown, G.W., Burn, G.L., Williamson, D.J., Pandžić, E., Peters, R., Holden, M., Ewers, H., Shao, L., Wiseman, P.W., and Owen, D.M. (2017). Live-cell super-resolution reveals F-actin and plasma membrane dynamics at the T cell synapse. Biophysical journal *112*, 1703-1713.

Cruzat, A., Witkin, D., Baniasadi, N., Zheng, L., Ciolino, J.B., Jurkunas, U.V., Chodosh, J., Pavan-Langston, D., Dana, R., and Hamrah, P. (2011). Inflammation and the nervous system: the connection in the cornea in patients with infectious keratitis. Investigative ophthalmology & visual science *52*, 5136-5143.

Di Girolamo, N., Bobba, S., Raviraj, V., Delic, N., Slapetova, I., Nicovich, P., Halliday, G., Wakefield, D., Whan, R., and Lyons, J. (2015). Tracing the fate of limbal epithelial progenitor cells in the murine cornea. Stem cells *33*, 157-169.

Grimm, V., Berger, U., DeAngelis, D.L., Polhill, J.G., Giske, J., and Railsback, S.F. (2010). The ODD protocol: a review and first update. Ecological modelling *221*, 2760-2768.

Lobo, E.P., Delic, N.C., Richardson, A., Raviraj, V., Halliday, G.M., Di Girolamo, N., Myerscough, M.R., and Lyons, J.G. (2016). Self-organized centripetal movement of corneal epithelium in the absence of external cues. Nature communications *7*.

Meddens, M.B., Pandzic, E., Slotman, J.A., Guillet, D., Joosten, B., Mennens, S., Paardekooper, L.M., Houtsmuller, A.B., Van Den Dries, K., and Wiseman, P.W. (2016). Actomyosin-dependent dynamic spatial patterns of cytoskeletal components drive mesoscale podosome organization. Nature communications *7*.

Richardson, A., Lobo, E.P., Delic, N.C., Myerscough, M.R., Lyons, J.G., Wakefield, D., and Di Girolamo, N. (2017). Keratin-14-Positive Precursor Cells Spawn a Population of Migratory Corneal Epithelia that Maintain Tissue Mass throughout Life. Stem Cell Reports *9*, 1081-1096.

Thoft, R.A., and Friend, J. (1983). The X, Y, Z hypothesis of corneal epithelial maintenance. Investigative ophthalmology & visual science *24*, 1442-1443.

1 Toplak, T., Pandzic, E., Chen, L., Vicente-Manzanares, M., Horwitz, A.R., and Wiseman, P.W. (2012). STICCS reveals
2 matrix-dependent adhesion slipping and gripping in migrating cells. Biophysical journal *103*, 1672-1682.